

# Comparison of spatial differencing schemes for the equation of radiative transfer applied to biomedical tissues

H. Kim\*, A Hielscher\*

Dept. of Biomedical Engineering, Columbia University  
New York, NY 10027

## ABSTRACT

When numerically implementing the equation of radiative transfer (ERT) to calculate light propagation in biological tissue, one has several choices on how to perform the spatial discretization. In this study we investigate the performance of two commonly employed differencing schemes (“step” and “weighted diamond”). Using a discrete-ordinates finite-volume method in a two-dimensional absorbing and scattering medium, the code performances are evaluated in terms of accuracy and computational requirement. We find that, compared to the step-differencing scheme, the weighted diamond differencing scheme provides more accurate solutions of the radiation intensity over a wide range of optical properties. Furthermore, the weighted diamond scheme is computationally more efficient than the step method. When used in conjunction with tomographic reconstruction algorithms, we observe that using the weighted-diamond differencing scheme leads to more accurate reconstructions of the optical properties.

**Keywords:** radiative transfer equation, spatial differencing scheme, step scheme, weighted diamond scheme, optical tomography.

## 1. INTRODUCTION

Near-infrared optical tomography (NIROT) is an emerging imaging modality that has been applied to a wide variety of biomedical fields<sup>1-2</sup>. This technique retrieves the spatial dependent distributions of optical properties, i.e., scattering and absorption coefficients, inside biological tissues by analyzing light intensities measured at boundary surfaces with a well-established model-based iterative image reconstruction (MOBIIR) schemes. The accurate forward modeling for predictions of radiation intensities at boundaries is a prerequisite for quality reconstruction. Initially the diffusion approximation<sup>3-4,7-8</sup> to the equation of radiative transfer (ERT) was commonly employed. This approximation, however, fails for cases of highly absorbing objects and when light transport in the void-like regions, such as the cerebrospinal or amniotic fluid, are considered.<sup>13-14</sup> To overcome these limitations, researchers have increasingly focused on directly solving the full equation of radiative transfer, and have further refined it into the time-dependent or time-independent or frequency-domain ERT versions<sup>9-12,15,16</sup>.

Thus radiative transfer through tissue-like media is now playing an important role in many biomedical applications such as optical tomography. Several solution methods have been developed for radiative transfer problems, including the zone, Monte Carlo, ray tracing, spherical harmonics, discrete transfer, discrete ordinates and finite volume methods<sup>17</sup>. Among them, the Monte Carlo, ray tracing and zone methods are the most accurate but their computational requirements are also the highest. Therefore, many researchers use the discrete-ordinates method,<sup>18,19</sup> which has shown to provide reasonably accurate solution at relatively small computational burden.

The accuracy of the discrete-ordinates method is mainly compromised by two factors: ray effects and false scattering<sup>20,21</sup>. The ray effect is associated with the angular discretization and arises from approximations of the continuous angular variation of the intensity field over the total solid angle by a discrete ordinates set of radiation intensities. Ray effects may be mitigated by increasing the number of angular directions or by modified discrete ordinates method<sup>22</sup>. The false scattering, which places a role in low-scattering, void-like regions, is closely connected with the spatial discretization and occasionally occurs when the rays are not aligned with the grid lines. Again, the use of fine meshes may reduce false scattering to some degree.

---

\* H. Kim: hkk2107@columbia.edu; phone 1-212-854-5737; fax 1-212-854-8725

\* A. Hielscher: ahh2004@columbia.edu; phone 1-212-854-5080; fax 1-212-854-8725

In the study at hand, we evaluate the spatial differencing schemes that strongly affect the solution accuracy in the discrete ordinates method. The two most popular spatial differencing schemes are the step and diamond differencing schemes. The great advantage of the step differencing scheme is that it always produces positive radiation intensities. However this scheme is only first-order accurate and has the disadvantage of introducing excessive false scattering. The diamond scheme can reduce false scattering to considerable degree, but may yield overshoots or undershoots of the radiation intensity at the boundary, and occasionally produces negative radiation intensities as reported in the literature. The occurrence of negative intensities can be eliminated by the fix-up procedure proposed in the literature<sup>23</sup>, which sets the negative intensities to zero whenever they appear. However spatial oscillation or physically unrealistic intensities may still occur. This problem can be overcome by using the positive scheme or weighted diamond scheme proposed by Lathrop<sup>24</sup> that combines the step and diamond schemes. Thus the performances of the two spatial differencing schemes have already been widely investigated for the cases of absorption-dominant media, but there is a lack of information regarding the performance of these schemes with tissue-like scattering media; which are the focus of this study.

In the following we apply to tissue-like media the two popular spatial differencing schemes (step and weighted diamond scheme) and investigate their performances associated with the solution accuracy and the computational requirements. Solutions obtained with these two approaches are compared to results obtained with a reference solution that is generated with a sufficient mesh refinement. Furthermore, effects of those schemes on the reconstruction accuracy are discussed. The discrete ordinates method is briefly introduced in the next section. Spatial differencing schemes employed in this work are described. Several test problems are solved for a two dimensional rectangular enclosure with an absorbing and scattering tissue-like medium.

## 2. THE DISCRETE ORDINATES FINITE VOLUME METHOD

### 2.1 Radiative transfer equation (RTE)

Consider the radiative transfer equation (RTE) in a Cartesian coordinate system as shown in Fig. 1a. The variation of the radiation intensity passing in a specified direction  $\Omega$  through a small control volume in an absorbing-scattering medium can be written as follows<sup>25</sup>

$$(\Omega \cdot \nabla)I(\mathbf{r}, \Omega) = -(\mu_a + \mu_s)I(\mathbf{r}, \Omega) + \frac{\mu_s}{4\pi} \int_{4\pi} I(\mathbf{r}, \Omega')\Phi(\Omega' \rightarrow \Omega)d\Omega \quad (1)$$

where  $I(\mathbf{r}, \Omega)$  is the radiation intensity, [W/cm<sup>2</sup>];  $\mu_a$  and  $\mu_s$  are the absorption and scattering coefficients [cm<sup>-1</sup>] of the medium, respectively, a function of position only;  $\Phi(\Omega' \rightarrow \Omega)$  is the scattering phase function from the incoming direction  $\Omega'$  into the outgoing direction  $\Omega$ . The Henyey-Greenstein phase function<sup>25</sup> widely used in tissue optics is chosen here as

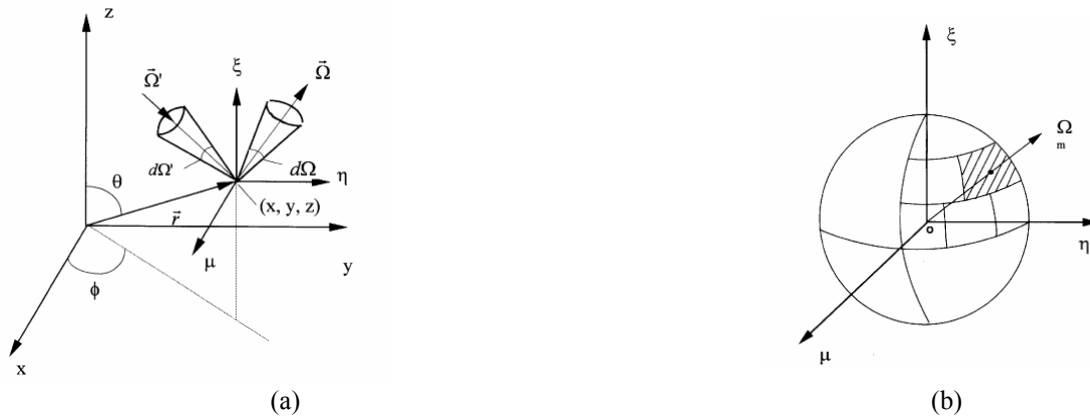


Fig. 1. Physical coordinates and angular discretization; (a) Cartesian coordinates; (b)  $S_N$ -type discretization

$$\Phi(\Omega' \rightarrow \Omega) = \frac{1 - g^2}{(1 + g^2 - 2g \cos \Theta)^{3/2}} \quad (2)$$

where  $\Theta$  is the angle between  $\Omega$  and  $\Omega'$  and  $g$  is the anisotropy factor which measures how peaked the scattering is. In order to treat anisotropic scattering, we renormalize the phase function according to the procedure of Kim and Charette<sup>26-27</sup>.

With an isotropic radiation source, the non-reentry boundary conditions can be given as

$$I(\mathbf{r}_w, \Omega) = \begin{cases} I_{in} & , \mathbf{n} \cdot \Omega < 0 \\ 0 & , \mathbf{n} \cdot \Omega > 0 \end{cases} \quad (3)$$

where  $I(\mathbf{r}_w, \Omega)$  is the intensity leaving from the boundary surface and traveling into the medium;  $I_{in}$  is the radiation source located on the surface;  $\mathbf{n}$  is the unit outward vector normal to the surface.

## 2.2 Angular discretization

The  $S_N$  quadrature scheme, as shown in Fig. 1b, is employed that fits well into the discrete ordinates method. With the  $S_N$  quadrature, the radiative transfer equation is replaced by the discrete set of  $M$  coupled differential equations that describe the radiation intensities along  $M$  discrete directions. Integrals over the  $4\pi$  solid angle is also replaced by the discrete set of  $M$  quadratures to give

$$\mu^m \frac{\partial I^m}{\partial x} + \eta^m \frac{\partial I^m}{\partial y} = -(\mu_a + \mu_s)I^m + \frac{\mu_s}{4\pi} \sum_{m'=1}^M I^{m'} \Phi(m', m) w_{m'} \quad (4)$$

where the superscript  $m$  represents the specified direction vector  $\Omega^m = (\mu^m, \eta^m, \xi^m)$  with the directional cosines corresponding to the  $x$ ,  $y$  and  $z$  Cartesian coordinates;  $w_{m'}$  are the quadrature weights for directions  $m'$  approximating the integrals over the solid angle.

## 2.3 Spatial discretization

Next, spatial discretization is performed to solve the coupled  $M$  discrete ordinates equations (4). According to the finite volume approach, equation (4) is integrated over the control volume as depicted in Fig. 2a, and a Gauss divergence theorem is applied to the spatial differentiation term. Especially the in-scattering term is split into two parts<sup>28</sup>: one that accounts for contribution of the  $m$ -th direction and the other accounting for all other directions.

After integration over the control volume, we obtain the final discretized form of the radiative transfer equation over the

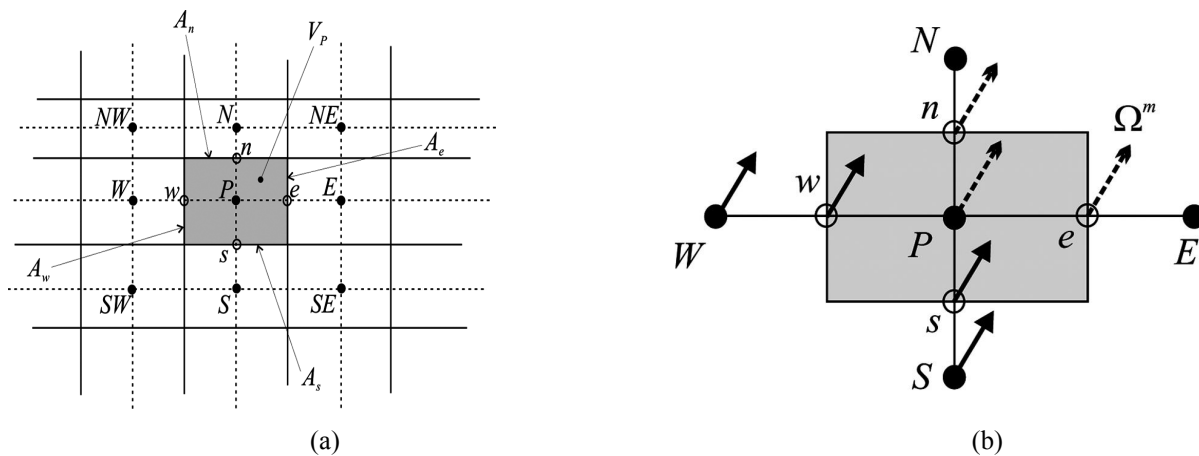


Fig. 2. Control volume and spatial differencing; (a) node description; (b) intensities in positive directional cosines

control volume  $\Delta V_p$  and the control angle (or discrete ordinates)  $\Delta\Omega^m$  as

$$\begin{aligned} & \left| \mu^m \right| A_x (I_{x,out}^m - I_{x,in}^m) + \left| \eta^m \right| A_y (I_{y,out}^m - I_{y,in}^m) \\ & = -(\beta I_p^m + S_p^m) \Delta V_p \end{aligned} \quad (5)$$

where  $A_x = A_e = A_w = \Delta y$  and  $A_y = A_n = A_s = \Delta x$  are the areas of the control volume surfaces normal to the  $x$  and  $y$  directions;  $\Delta V_p (= \Delta x \cdot \Delta y)$  is the control volume over which the integration is carried out; the modified extinction coefficient is introduced as

$$\beta = \mu_a + \mu_s - \frac{\mu_s}{4\pi} I_p^m \Phi(m, m) w_m \quad (6)$$

which is intended to accelerate the iterative solution procedure, and the modified source term is also given for the nodal point  $P$  and the discrete direction  $m$ .

$$S_p^m = \frac{\mu_s}{4\pi} \sum_{\substack{m'=1 \\ (m' \neq m)}}^M I_p^{m'} \Phi(m', m) w_{m'}. \quad (7)$$

The subscripts for intensities at the control volume surfaces denote the direction ( $x$  and  $y$  directions) and the upstream ( $in$ ) and the downstream face ( $out$ ). If  $\mu^m > 0$ , then  $I_{x,in}^m$  and  $I_{x,out}^m$  are the intensities at the west and east cell faces, respectively. Conversely, if  $\mu^m < 0$ , then  $I_{x,in}^m$  and  $I_{x,out}^m$  are the intensities at the east and west cell faces, respectively. The radiation intensities at the cell faces are unknowns and must be related to radiation intensities at neighboring grid nodes. This relationship makes the difference between the step and the weighed diamond differencing schemes.

## 2.4 Step differencing scheme

In the step differencing scheme, the downstream surface intensities are replaced by the upstream nodal intensities. As mentioned earlier, this scheme has often been applied to Cartesian coordinate grids, in order to avoid negative intensities that could occur with schemes such as diamond one.

For  $\mu^m > 0$  and  $\eta^m > 0$  directions as shown in Fig. 2b, equation (5) gives the radiation intensity at nodal point  $P$  as

$$I_p^m = \frac{\left| \mu^m \right| A_w I_w^m + \left| \eta^m \right| A_s I_s^m + S_p^m \Delta V_p}{\left| \mu^m \right| A_w + \left| \eta^m \right| A_s + \beta_p \Delta V_p}. \quad (8)$$

The downstream intensities are set equal to be the upstream nodal intensity as  $I_e^m = I_n^m = I_p^m$ . Similarly, we can obtain the relations between the nodal intensity and the surface intensities for other directions, although not repeated here.

## 2.5 Weighted diamond differencing scheme

A weighted spatial differencing scheme relates the radiation intensities on cell surfaces with those on cell centers as

$$I_p^m = (1 - f_x^m) I_w^m + f_x^m I_e^m = (1 - f_y^m) I_s^m + f_y^m I_n^m \quad (9)$$

where  $f_{x(y)}^m$  is a weighting factor between 0.5 and 1. The subscript denotes the surface elements,  $x$  and  $y$ . In general, the spatial differencing with  $f_{x(y)}^m = 0.5$  is the diamond scheme of the second order accuracy, while the one with  $f_{x(y)}^m = 1$  is the step differencing scheme of the first order accuracy. To overcome the shortcomings of the regular diamond scheme such as negative intensities or under-shooting, as mentioned earlier, we employ here the variable

weighted diamond scheme proposed by Lathrop<sup>24</sup> that guarantees positive intensities with the weighting factors given in terms of the spatial and angular grid, and the total extinction coefficient. According to the procedure of Lathrop, the weighting factors are given in two dimensions as

$$f_x^m = \max\left(1 - \frac{D_x^m}{2D_y^m + \beta_p \Delta V}, 0.5\right) \text{ and } f_y^m = \max\left(1 - \frac{D_y^m}{2D_x^m + \beta_p \Delta V}, 0.5\right) \quad (10)$$

where

$$D_x^m = |\mu^m| A_x \text{ and } D_y^m = |\eta^m| A_y \quad (11)$$

For  $\mu^m > 0$  and  $\eta^m > 0$  directions, equation (5) can be reformulated with the weighting factors (10) as

$$I_p^m = \frac{\frac{|\mu^m| A_w}{f_x^m} I_w^m + \frac{|\eta^m| A_s}{f_y^m} I_s^m + S_p^m \Delta V_p}{\frac{|\mu^m| A_w}{f_x^m} + \frac{|\eta^m| A_s}{f_y^m} + \beta_p \Delta V_p} \quad (12)$$

If  $I_w^m$  and  $I_s^m$  are assumed to be known, where the iteration is done in a direction of positive directional cosines, then the nodal intensity  $I_p^m$  is calculated by using (12) and the interface intensities  $I_e^m$  and  $I_n^m$  are also obtained with the relations (9).

## 2.6 Iterative solution procedure

Solution of equation (12) requires an iterative procedure since the radiation intensities are strongly coupled through the source term  $S_p^m$  that is function of the unknown cell center intensities in different directions. The more detailed solution procedure may be found elsewhere<sup>29</sup>. An intensity solution is obtained when the following convergence criterion is satisfied:

$$\max_{\text{all unknowns}} \left( \left| \frac{I_p^{new} - I_p^{old}}{I_p^{old}} \right| \right) \leq 10^{-6} \quad (13)$$

The incident radiation and the radiative flux are obtained as

$$G_p = \int_{4\pi} I(\mathbf{r}, \Omega) d\Omega \text{ and } Q_{r_w} = \int_{\mathbf{n} \cdot \Omega > 0} I(\mathbf{r}_w, \Omega) (\mathbf{n} \cdot \Omega) d\Omega \quad (14)$$

where  $\mathbf{r}_w$  denotes the location of evaluation at boundaries.

## 3. RESULTS AND DISCUSSIONS

We first use the step and weighted-diamond differencing schemes to predict radiation intensities inside a homogeneous absorbing-scattering medium. A 1-cm by 1-cm test medium is illuminated by a radiation source located at position (0, 0.5cm) on the boundary surface. The incident radiation  $G_p$  and the radiative flux  $Q_r$  as defined in (14) are evaluated to address the performances of the two schemes. The reference solutions are generated with a sufficient mesh refinement by using the hybrid scheme<sup>30</sup> which has been known to be more accurate than the step scheme. It is also known that the hybrid scheme performs very similarly to the weighted diamond scheme in both accuracy and computation time since it is theoretically and conceptually similar to the weighted diamond scheme. This is why the hybrid scheme is not compared in this study with the other two schemes and only used for the reference solution. In comparison to the reference solution, the accuracy of each scheme is measured as follows:

Table 1. Descriptions for the cases considered; optical properties of each medium and the numbers of nodal points and  $S_N$  quadratures used for the reference and simulation data, and the errors of incident radiances and boundary radiation fluxes predicted by the two spatial differencing schemes. Also the weighting factors in a diagonal direction are given for the weighted diamond scheme.

Case	Optical properties		$g$	$S_N$	No. of nodes		Step scheme		Weighted scheme			
	$\mu_a$ [cm <sup>-1</sup> ]	$\mu_s$ [cm <sup>-1</sup> ]			reference	simulation	$E_G$	$E_Q$	$E_G$	$E_Q$	$f_x$	$f_y$
1	0.01	10	0	$S_8$	167×167	57×57	2.0826	2.3102	2.0085	2.0363	5.681	5.681
2	0.5	10	0	$S_8$	167×167	57×57	2.3482	2.6237	2.0160	2.0408	5.709	5.709
3	1.0	10	0	$S_8$	167×167	57×57	2.5616	2.8884	2.0142	2.0357	5.738	5.738
4	0.01	20	0	$S_8$	335×335	113×113	2.0734	2.3542	2.0017	2.0305	5.675	5.675
5	0.01	50	0	$S_8$	755×755	253×253	2.0777	2.4370	1.9999	2.0313	5.735	5.735
6	0.01	20	0.5	$S_{12}$	335×335	113×113	2.0408	2.1701	2.0017	2.0186	5.823	5.823
7	0.5	50	0.8	$S_{12}$	755×755	253×253	2.0284	2.1120	2.0013	2.0125	6.660	6.660

$$E_G = \frac{1}{N_G} \sum_{i=1}^{N_G} \left| \frac{G_{P_i}^s - G_{P_i}^r}{G_{P_i}^r} \right|, \text{ and } E_Q = \frac{1}{N_Q} \sum_{i=1}^{N_Q} \left| \frac{Q_{r_i}^s - Q_{r_i}^r}{Q_{r_i}^r} \right| \quad (15)$$

where  $E_Q$  and  $E_G$  denote the errors for the incident radiance  $G_P$  and the radiative flux  $Q_r$ , respectively;  $N_G$  and  $N_Q$  denote the numbers of evaluation points for  $G_P$  and  $Q_r$  respectively.

### 3.1 Effects of false scattering

The effect of false scattering on the intensity accuracy is first investigated with the two schemes. In this respect, we consider the low-absorbing and low-scattering medium to mimic the void-like regions in tissues. A 57 x 57 grid system is used with a  $S_8$  ordinates set. Fig. 3 shows the intensity distribution for a diagonal direction of grid from the two spatial differencing schemes. As expected, the weighted diamond scheme (Fig. 3b) includes little false scattering and predicts more accurate results, while the step scheme (Fig. 3a) shows severe smearing due to strong false scattering. However, when considering the edge direction of the control volume, it is observed that the step scheme show little false scattering while the weighted diamond scheme exhibits very weak false scattering, although not shown in figure. Thus even to the weighted diamond scheme it may not be possible to completely eliminate false scattering in all directions.

### 3.2 Low absorbing and variable scattering media

We start with the case where the absorption and scattering coefficients are  $\mu_a=0.01$ [1/cm] and  $\mu_s=10$ [1/cm]. Note that the medium is isotropic-scattering. The numerical experiments are performed by varying the absorption coefficient only from 0.01 [1/cm] to 0.5 [1/cm] with the scattering coefficient fixed as  $\mu_s=10$ [1/cm]. The 57 by 57 grid and a  $S_8$  ordinates set are used for analysis. Incident radiances  $G_P$  and radiative fluxes  $Q_r$  are obtained at interior and boundary points,

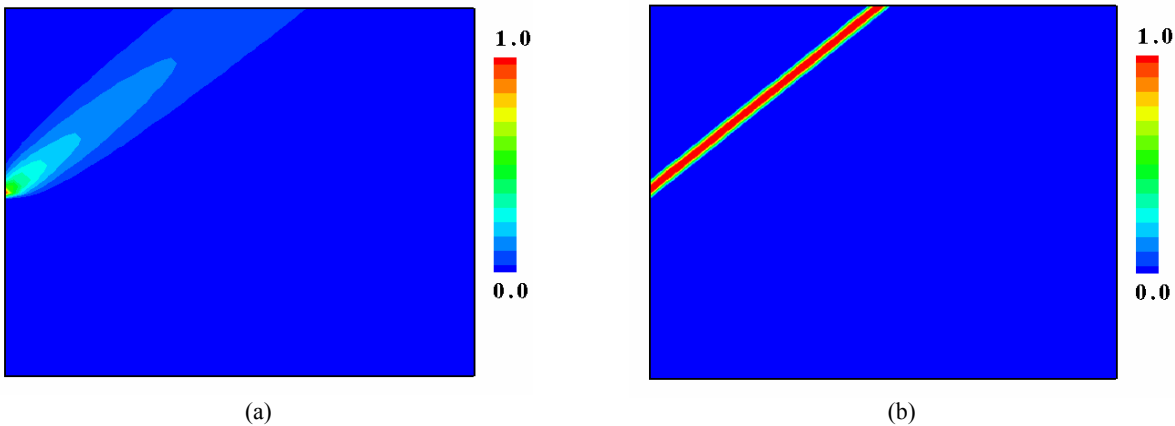


Fig. 3. Intensity distribution in a specified direction ( $\mu_t=0.57735$ ,  $\eta_t=0.57735$ ) obtained with the two spatial differencing schemes for case of  $\mu_a=0.01$ [1/cm] and  $\mu_s=0.01$ [1/cm]: (a) step scheme; (b) weighted diamond scheme.

Table 2. Weighting factors of the weighted diamond scheme in a diagonal direction obtained with varying the scattering coefficient while the absorption coefficient is fixed with the mesh size.

Optical properties		$g$	$S_N$	No. of nodes	Weighted scheme	
$\mu_a$ [ $\text{cm}^{-1}$ ]	$\mu_s$ [ $\text{cm}^{-1}$ ]				$f_x$	$f_y$
0.01	10	0	$S_8$	$57 \times 57$	5.681	5.681
0.01	20	0	$S_8$	$57 \times 57$	6.198	6.198
0.01	30	0	$S_8$	$57 \times 57$	6.604	6.604
0.01	40	0	$S_8$	$57 \times 57$	6.932	6.932
0.01	50	0	$S_8$	$57 \times 57$	7.203	7.203

respectively, and compared with the reference solution to examine the accuracy of the two schemes. The errors with the two schemes are given in Table 1 with their absolute values. On the whole, both schemes exhibit larger errors in the prediction of the radiative flux rather  $Q_r$  than the incident radiance  $G_p$ . Also it is shown from cases 1, 2 and 3 that the error of the step difference scheme increases rapidly as the absorption coefficient increases while the accuracy of the weighted diamond scheme is very slightly sacrificed by increasing the absorption coefficient. This behavior can be explained by examining the weighting factors of the weighted diamond scheme because the accuracy of the scheme is directly affected by such factors. The corresponding factors for the cases considered here are given in Table 1. It is not hard to find that, in spite of increased absorption coefficient, the weighting factors of the weighted diamond scheme are still around 0.5 which ensures second-order accuracy. On the other hand, the step scheme essentially requires the mesh refinement for reasonable accuracy.

Fig.4 shows the distributions of radiative fluxes for case 3 with  $\mu_a=1[1/\text{cm}]$  and  $\mu_s=10[1/\text{cm}]$ . In both schemes, the predictions are highly overestimated over the reference solution, which results from the fact that the schemes are tested somewhat on the coarser grids as compared with the reference. However, it should be noted that the weighted diamond scheme predicts much closer results to the reference than the step scheme. Also it is shown from Fig. 4b that the results from both schemes converge to the reference solution as the mesh size gets smaller.

### 3.3 Low scattering and variable absorbing media

Here we increase the scattering coefficient from 10 to 20 to 50  $[1/\text{cm}]$  and see the characteristics of the schemes with respect to the accuracy. At this time, the absorption coefficient is fixed to be 0.01  $[1/\text{cm}]$ . According to the strength of scattering, the spatial mesh is properly refined to capture the scattering events in the simulations. The errors of incident radiances and radiative fluxes are given for cases 1, 4 and 5 in Table 1. As before, the weighted diamond scheme seems more accurate but local radiation fluxes predicted by the two schemes still exhibit large errors as compared with the reference data. This discrepancy is also observed at predictions of incident radiances. A careful look at cases 1, 4 and 5 in Table 1 indicates that each of the schemes maintains the same order of accuracy for each case. This is expected because: for the step scheme the mesh refinement is made to compromise the error due to increased scattering coefficient and for same reason the weighted scheme keeps its weighting factors around 0.5 as in Table 1. Then the next question



Fig. 4. Local radiative fluxes obtained with the two schemes for case 4 with  $\mu_a=1[1/\text{cm}]$  and  $\mu_s=10[1/\text{cm}]$ : (a) coarse mesh; (b) mesh refinement.

Table 3. Reconstruction problems considered with the two schemes

Problem	Anisotropic factor	Background		Object	
		$\mu_a$ [1/cm]	$\mu_s$ [1/cm]	$\mu_a$ [1/cm]	$\mu_s$ [1/cm]
1	0.5	0.1	10	0.2	10
2	0.0	0.5	10	0.6	10
3	0.8	0.5	50	0.6	50

will be what if the scattering coefficient only is increased. From Table 2, for the fixed mesh size the weighting factors are found to increase with the scattering coefficient. This means the accuracy of the weighted diamond scheme gradually degrades and finally becomes identical to that of the step scheme.

Now we address effects of anisotropic scattering on the accuracy of the two schemes. The optical properties of the medium is  $\mu_a=0.01$ [1/cm] and  $\mu_s=20$ [1/cm] with  $g=0.5$ . To simulate the anisotropic events of scattering, the higher-order angular quadrature ( $S_{J2}$ ) is used and the spatial domain is also covered with smaller meshes. In comparison to isotropic scattering (case 4), it is shown that both of the two schemes produce somewhat better results in anisotropic scattering in both radiative fluxes and incident radiances. This improvement is made possible by the forward scattering characteristic of the medium. In other words, forward scattering can be thought of reduced isotropic scattering which may be favorable to the accuracy of the scheme. Based on the results so far, we can say that the accuracy of the weighted diamond scheme is solely affected by the weighting factors which are more sensitive to change in the scattering coefficient than in the absorption coefficient.

Additionally, we compare the two spatial differencing schemes with each other in terms of computational requirements. We found that on the same mesh, the weighted diamond scheme takes longer computation time than the step differencing scheme. This is true because the step differencing scheme eliminates the interface intensities by simply replacing them by the upstream cell-center intensities, while the weighted diamond scheme has to compute the interface intensities by using the cell-center intensities obtained through an iterative procedure. Therefore the weighted diamond scheme takes more iteration to converge. In terms of same accuracy, however, the step scheme takes more computation time as it requires refined meshes to be as accurate as the weighted diamond scheme. Indeed it is found that the weighted diamond scheme is faster by a factor of at least 2.3 than the step scheme.

### 3.4 Applications to absorption reconstruction

We also investigated the effect of the two spatial differencing schemes on tomographic reconstruction results, especially the retrieval of a spatially dependent absorption coefficient. Four sources are located at surface centers of the medium boundary and radiation fluxes are predicted at detectors positions on the surfaces. The hybrid scheme is used to generate the synthetic data while the step and weighted diamond schemes are used into the forward model for reconstruction. All forward runs are performed on a 40 by 40 mesh with a  $S_8$  quadrature. The target medium has one object which exists within  $0.2 \leq x \leq 0.5$  and  $0.2 \leq y \leq 0.4$ . The object differs only in the absorption coefficient, i.e., the scattering coefficient of the object is equal to that of the background medium. The absorption coefficient is retrieved by minimizing

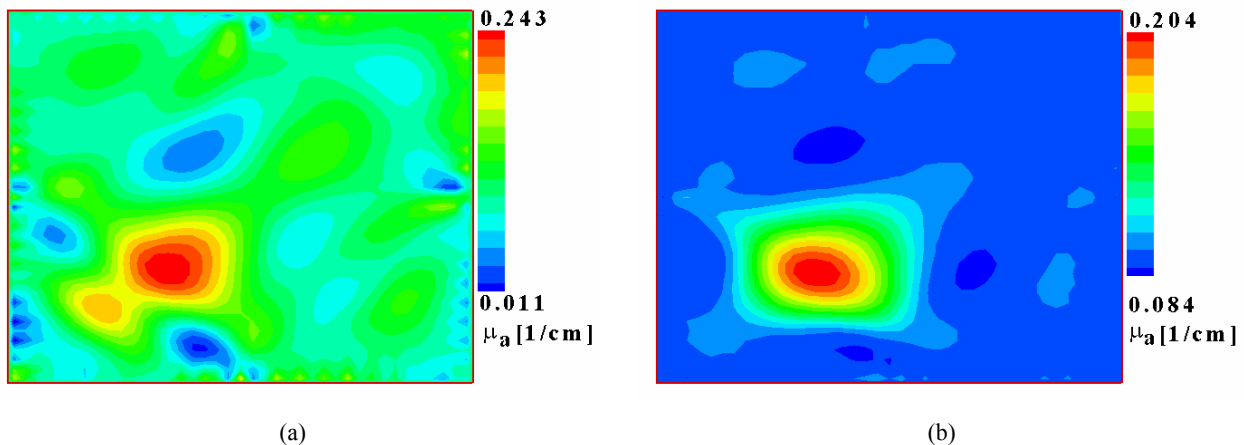


Fig. 5. Reconstruction maps of absorption coefficients obtained for problem 1 with the two schemes; (a) step scheme; (b) weighted diamond scheme.

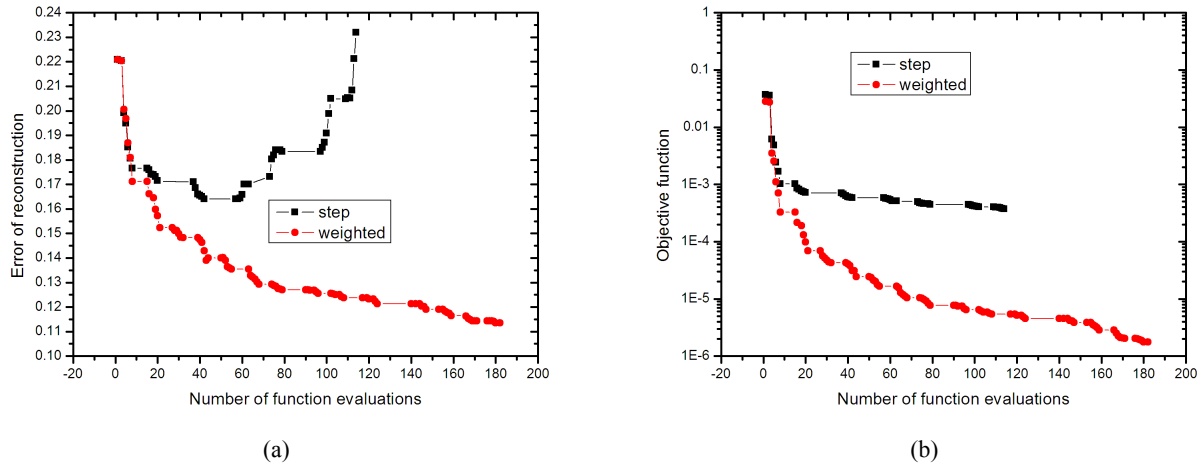


Fig. 6. Variations of the accuracy and the value of objective function with respect to function evaluations; (a) accuracy; (b) objective function value.

the discrepancies between the measured and predicted intensities through an lm-BFGS method<sup>31</sup>. To investigate effects of the two spatial schemes on the image accuracy of reconstruction, we consider three test problems as given in Table 3. To proceed with reconstructions, we set the initial guess to be equal to the absorption coefficient of the background medium.

Fig.5 shows the reconstructed maps of the absorption coefficient with respect to the two schemes. The step scheme overestimates the optical properties of the medium and gets artifacts around the object, while the weighted diamond scheme retrieves the absorption coefficient accurately. This is because the step scheme tends to overestimate the radiation fluxes at boundaries. In other words, the step scheme gives rise to overestimation in intensities which consequently leads to excessive increase in the absorption coefficient as the reconstruction scheme minimizes the difference between predictions and measurements. Also we examine characteristics of the two schemes with respect to reconstruction error and convergence rate. As shown in Fig. 6, whereas the step scheme tends to increase the reconstruction error after certain error level (see Fig. 6a), the weighted diamond scheme shows steady decrease in the error. Also the step scheme gives rise to pre-matured convergence (see Fig. 6b). As for the other two cases, the reconstruction accuracy from the two schemes is found to depend upon the optical properties of the medium. To be specific, the two schemes show similar reconstruction characteristics in higher scattering media than otherwise, as shown in Fig. 7-8. In brief, the reconstructed maps obtained with the weighted diamond differencing scheme give more accurate results than the step differencing scheme. It is also observed that the step scheme overestimates the absorption coefficient of the object.

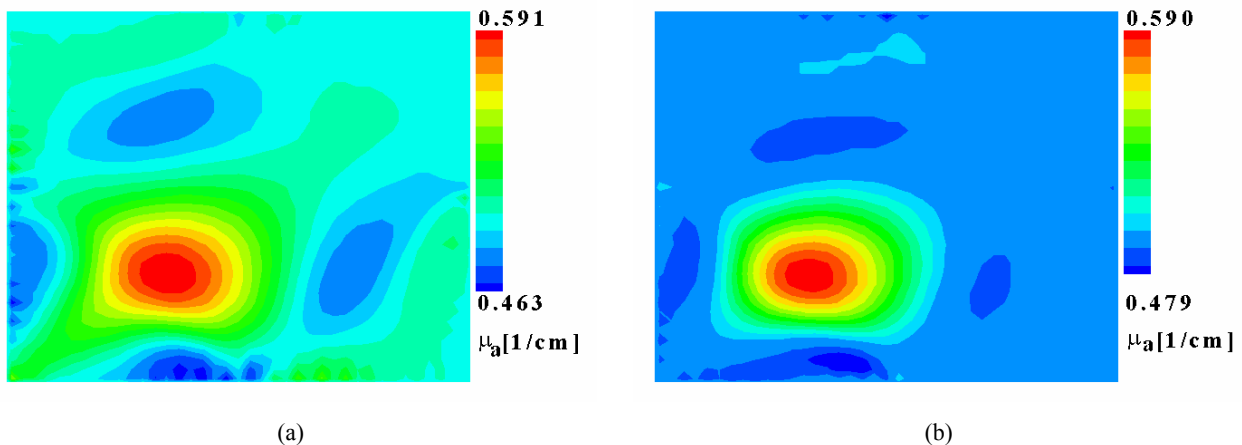


Fig. 7. Reconstruction maps of absorption coefficients obtained for problem 2 with the two schemes; (a) step scheme; (b) weighted diamond scheme.

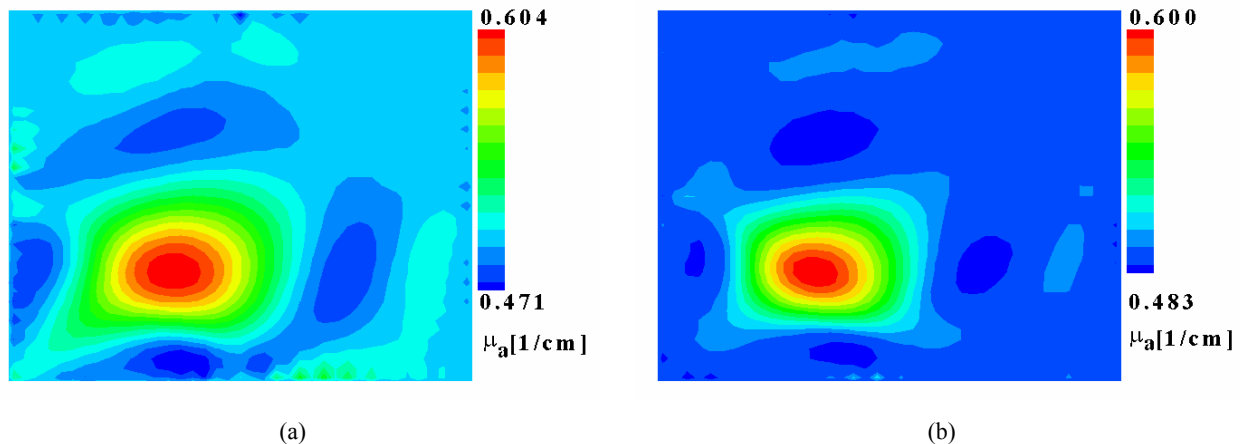


Fig. 8. Reconstruction maps of absorption coefficients obtained for problem 3 with the two schemes; (a) step scheme; (b) weighted diamond scheme.

#### 4. SUMMARY AND CONCLUSIONS

In this study, we have tested and compared the performance of two spatial differencing schemes (step and weighted-diamond) which are commonly employed in numerical implementation of the equation of radiative transfer (ERT). In conjunction with a discrete-ordinates finite-volume method these schemes provide predictions of the radiation intensity in absorbing and scattering media. We have considered several test media and the radiation intensities obtained with these two schemes are compared with the reference solutions. Also effects of these two schemes on the reconstruction of the absorption coefficient have been investigated with numerical simulations. The following conclusions have been obtained:

In forward simulations, the weighted diamond differencing scheme produces more accurate results over all range of optical properties considered here, since it can reduce false scattering that occurs in the step scheme. It has also been found that the accuracy of the weighted diamond scheme depends upon the strength of the total extinction coefficient of the medium rather than upon either absorption or scattering coefficients. On the other hand, the step scheme gives overshooting of intensity caused by false scattering, with larger error for higher absorbing media. In terms of computational requirement, the weighted diamond scheme is superior to the step scheme that requires finer meshes to secure the same accuracy as in the weighted diamond scheme.

In optical tomographic reconstruction, the use of the weighted-diamond scheme gives closer reconstruction results to the exact map. The step differencing scheme tends to produce overestimation of absorption coefficient due to overestimation in intensity. In conclusion, it is demonstrated that the use of weighted diamond differencing scheme can significantly contribute not only to the improved accuracy but also to the computational efficiency.

#### ACKNOWLEDGEMENTS

This work was supported in part by grants from the National Institute of Arthritis and Musculoskeletal and Skin Diseases (NIAMS-2R01-AR046255) and the National Institute of Biomedical Imaging and Bioengineering (NIBIB-R01EB001900), which are both divisions of the National Institutes of Health (NIH). Furthermore, the New York State Office of Science, Technology and Academic Research (NYSTAR) supported this work through their Technology Transfer Incentive Program (TTIP, grant # C020041).

#### REFERENCES

1. A.Y. Bluestone, G. Abdoulaev, C.H. Schmitz, R.L. Barbour and A.H. Hielscher, "Three-dimensional optical tomography of hemodynamics in the human head", *Optics Express* 9, 272-286(2001).

2. S. Nioka, Y. Yung, M. Shnall S. Zhao, S. Orel, C. Xie, B. Chance and L. Solin, "Optical imaging of breast tumor by means of continuous waves", *Adv. Exp. Med. Biol.* 411, 227-232(1997).
3. M.A. O'Leary, D.A Boas, B. Chance and A.G Yodh, "Experimental images of heterogeneous turbid media by frequency-domain diffusion photon tomography", *Opt. Lett.* 20, 426-428(1995).
4. M.S. Patterson, "Optical image reconstruction using frequency domain data: Simulations and experiments", *J. Opt. Soc. Am. A* 13, 253-266(1996).
5. A.D. Klose and A.H. Hielscher, "Quasi-newton methods in optical tomographic image reconstruction", *Inverse Problems* 19, 387-309(2003).
6. A.H. Hielscher, A.D. Klose and K.M. Hanson, "Gradient-based iterative image reconstruction scheme for time-resolved optical tomography", *IEEE Trans. Med. Imaging* 18, 262-271(1999).
7. R. Roy and E.M. Sevick-Muraca, "Truncated Newton's optimization scheme for absorption and fluorescence optical tomography. Part I: theory and formulation", *Optics Express* 4, 353-371(1999).
8. S.R. Arridge and M. Schweiger, "A gradient-based optimisation scheme for optical tomography", *Optics Express* 2, 213-226(1998).
9. A.D. Klose and A.H. Hielscher, "Optical tomography using the time-independent equation of radiative transfer-part 2: inverse model", *JQSRT* 72, 715-732(2002).
10. A.D. Klose and A.H. Hielscher, "Iterative reconstruction scheme for optical tomography based on the equation of radiative transfer", *Med. Phys.* 26, 1698-1707(1999).
11. J. Boulanger and A. Charette, "Numerical developments for short-pulsed near infra-red spectroscopy. Part I: direct treatment". *JQSRT* 91, 189-209(2005).
12. J. Boulanger and A. Charette, "Numerical developments for short-pulsed near infra-red spectroscopy. Part II: inverse treatment". *JQSRT* 91, 297-318(2005).
13. A.H. Hielscher, A.E. Alcouffe and R.L. Barbour, "Comparison of finite-difference transport and diffusion calculations for photon migration in homogeneous and heterogeneous tissues", *Phys. Med. Biol.* 43, 1285-1302(1998).
14. M. Firbank, S.R. Arridge, M. Schweiger and D.T. Delpy, "An investigation of light transport through scattering bodies with non-scattering regions", *Phys. Med. Biol.* 41, 767-783(1996).
15. K. Ren, G.S. Abdoulaev, G. Bal and A.H. Hielsher, "Algorithm for solving the equation of radiative transfer in the frequency domain", *Optics Letters* 29, 578-580(2004).
16. G. Abdoulaev, K. Ren and A. Hielsher, "Optical tomography as a PDE-constrained optimization problem", *Inverse Problems* 21, 1507-1530(2005).
17. R. Viskanta and M. P. Menguc, "Radiation heat transfer in combustion systems", *Prog. Energy Combust. Sci.* 13, 97 (1987).
18. B. G. Carlson and K. D. Lathrop, Transport theory—The method of discrete-ordinates, in *Computing Methods in Reactor Physics*, edited by H. Greenspan, C. N.Kelber, and D. Okrent, Gordon&Breach, NewYork, 1968.
19. W. A. Fiveland, "Discrete-ordinates solution of the radiative transport equation for rectangular enclosures", *J. Heat Transfer* 106, 699 (1984).
20. K. D. Lathrop, "Ray effects in discrete ordinates equations", *Nucl. Sci. Eng.* 32, 357 (1968).
21. J. C. Chai, H. S. Lee, and S. V. Patankar, "Ray effect and false scattering in the discrete ordinates method", *Numer. Heat Transfer B* 24, 373 (1993).
22. M. A. Ramankutty and A. L. Crosbie, "Modified discrete ordinates solution of radiative transfer in twodimensional rectangular enclosures", *J. Quant. Spectrosc. Radiat. Transfer* 57, 107 (1997).
23. K.D. Lathrop and B.G. Carlson, "Numerical solution of the Boltzmann transport equation", *Journal of Computational Physics* 2, 173-197(1967).
24. K.D. Lathrop, "Spatial differencing of the transport equation: positivity vs. accuracy", *Journal of Computational Physics* 4, 475-478(1969).

25. M. F. Modest, Radiative Heat Transfer, McGraw-Hill, New York, 1993.
26. H.K. Kim and A. Charette, "A sensitivity function-based conjugate gradient method for frequency domain optical tomography based on the equation of radiative transfer", *JQSRT* 104(1), 24-39(2007).
27. H.K. Kim and A. Charette, "Frequency domain optical tomography using a conjugate gradient method without line search", *JQSRT* 104(2),248-256(2007).
28. J.C. Chai, H.S. Lee and S.V. Patankar, "Improved treatment of scattering using the discrete ordinates method", *ASME J. Heat Transfer* 116, 260-263(1994).
29. W.A. Fiveland, "Three-dimensional radiative heat transfer solutions by the discrete ordinates method", *J. Thermophysics. Heat Transfer* 2(4), 309-316(1988).
30. I.K. Kim and W.S. Kim, "A hybrid spatial differencing scheme for discrete ordinates method in 2D rectangular enclosures", *International Journal of Heat and Mass Transfer* 44, 575-586(2001).
31. J. Nocedal and S.J. Wright, *Numerical optimization*, Springer, New York, 1999.